Nanoscale Advances

ROYAL SOCIETY OF CHEMISTRY

PAPER

View Article Online
View Journal | View Issue

Cite this: *Nanoscale Adv.*, 2023, **5**, 4819

Modeling and simulation for Cattaneo–Christov heat analysis of entropy optimized hybrid nanomaterial flow

Aneeta Razaq, *[a] Tasawar Hayat,[a] Sohail A. Khan *[a] and Ahmed Alsaedi [b]

Received 25th June 2023
Accepted 7th August 2023

DOI: 10.1039/d3na00453h

rsc.li/nanoscale-advances

Here, the hydromagnetic entropy optimized flow of a hybrid (Pb + $Fe_2O_3/C_2H_6O_2$) nanoliquid by a curved stretchable surface is addressed. The Darcy–Forchheimer model is utilized for porous space. Lead (Pb) and ferric oxide (Fe_2O_3) are considered the nanoparticles and ethylene glycol ($C_2H_6O_2$) as the base liquid. Thermal expression consists of dissipation and ohmic heating. Entropy generation is under consideration. The Cattaneo–Christov heat flux impact is discussed. Non-dimensional partial expressions by adequate transformations have been reduced to ordinary differential systems. The ND-solve technique is implemented for numerical solutions of dimensionless systems. Graphical illustrations of velocity, thermal field and entropy against influential variables for both nanoliquid ($Pb/C_2H_6O_2$) and hybrid nanoliquid (Pb + $Fe_2O_3/C_2H_6O_2$) are presented. Graphical illustrations of velocity, thermal field and entropy against sundry variables for both nanoliquid ($Pb/C_2H_6O_2$) and hybrid nanoliquid (Pb + $Fe_2O_3/C_2H_6O_2$) are presented. Influences of sundry variables on the Nusselt number and drag force for both nanoliquid ($Pb/C_2H_6O_2$) and hybrid nanoliquid (Pb + $Fe_2O_3/C_2H_6O_2$) are examined. A higher thermal relaxation time tends to intensify the heat transport rate and temperature. An increment in the magnetic variable leads to an enhancement of the entropy and thermal field. An improvement in liquid flow is seen for volume fraction variables. Velocity against the porosity variable and Forchheimer number is reduced. The Brinkman number leads to maximization of entropy generation.

1. Introduction

During the past few decades, hybrid nano-fluids have become popular among researchers, scientists and engineers due to their superior heat transport properties. Hybrid nano-fluids are suspensions of two or more nano-particles in the base fluid. The heat conductive performance of convectional materials (like blood, water, engine oil, ethylene glycol, *etc.*) can be enhanced by inserting nano-particles (like silica, carbon nanotubes, silver alumina, gold, lead, ferric oxide, *etc.*). Hybrid nano-fluids possess higher thermal conductivity for heat transfer phenomena such as those relevant to engines, vehicle radiators, machining, biomedicine, warming procedure on buildings, hybrid powered engines, pharmaceutical industries, paper production and many others. The concept of heat transport enhancement of the base liquid through addition of nano-particles was initially given by Choi and Eastman *et al.*[1,2] Hassan *et al.*[3] examined the partial slip effect for the flow of hybrid ferro-liquids. Radiation and porous space effects were addressed. Chabani *et al.*[4] examined the electrically conducting hybrid ($Ag–Al_2O_3/H_2O$) nanomaterial flow inside a modified trapezoidal permeable enclosure. Thermal transport analysis for hybrid nanoliquids with suction/injection in a rotating system was reported by Abdollahi *et al.*[5] Cattaneo–Christov analysis in the magnetohydrodynamic flow of ternary nano-materials with nonlinear radiation was studied by Alqawasmi *et al.*[6] Few latest developments related to hybrid nano-fluid flow under different geometric configurations are given in ref. 7–15.

Heat transfer is induced in view of temperature differences and subsequent temperature changes and distribution in different bodies. Heat transfer plays a significant role in industries, and biomedical and engineering processes such as those relevant to heat exchangers, air conditioning, refrigeration, equipment power collectors, fuel cells, drug targeting, microelectronics, heat conduction in tissues, *etc.* The mechanism of heat transfer was initially given by Fourier.[16] Fourier's law through parabolic expression predicts the infinite speed of heat waves. It is not acceptable physically. Therefore the thermal relaxation time was taken into account by Cattaneo.[17] For material invariant formulation to the Cattaneo's frame work Christov[18] introduced Oldroyd's upper convected derivative. Razaq *et al.*[19] explored the convective flow of the Reiner–Rivlin fluid subject to Cattaneo–Christov fluxes and MHD. Radiation impact for the magnetized flow of Prandtl nanoliquid with Cattaneo–Christov fluxes theory was given by Salmi *et al.*[20]

[a]*Department of Mathematics, Quaid-I-Azam University, 45320, Islamabad 44000, Pakistan. E-mail: arazaq@math.qau.edu.pk; sohailahmadkhan93@gmail.com*
[b]*Nonlinear Analysis and Applied Mathematics (NAAM) Research Group, Faculty of Science, King Abdulaziz University, P. O. Box 80207, Jeddah 21589, Saudi Arabia*

Haneef *et al.*[21] analyzed heat transport for Oldroyd-B material flow with Cattaneo–Christov fluxes. Random motion and thermophoresis effects in magnetohydrodynamic Oldroyd-B nanoliquid flow were studied by Hayat *et al.*[22] Latest articles for Cattaneo–Christov heat and mass fluxes are mentioned in ref. 23–28.

Entropy minimization (EM) optimizes thermal system performance by exploring associated irreversibility through heat and mass transfer, Joule heating and liquid friction. Entropy is a measure of uncertainty and disorderness of a system and its surroundings. All natural processes are thermodynamically irreversible. Entropy is inversely proportional to the temperature of a system. Entropy has a direct proportion to the reversible change in heat. Entropy generation is the loss of energy in thermodynamical systems due to diffusion processes, temperature difference, electric resistance, fluid mixing, chemical reaction, radiation and resistive forces. Applications of entropy generation are found in electronic cooling systems, geothermal reservoirs, thermal and nuclear reactors and heat exchanger pumps. Entropy optimization in thermally convection flow was studied in Bejan.[29–31] Iftikhar *et al.*[32] analyzed entropy generation for non-Newtonian biviscosity fluid in a square cavity. Hayat *et al.*[33] addressed the magnetized entropy optimized flow of the Reiner–Rivlin material. Maiti *et al.*[34] reported entropy generation analysis for time-dependent hybrid nanoliquid flow by shrinking a disk. Latest investigations for entropy analysis are highlighted in studies.[35–42]

This communication discusses the magnetohydrodynamic Darcy–Forchheimer flow of a hybrid nanomaterial. The Cattaneo–Christov heat relation is under consideration. Ferric oxide (Fe_2O_3) and lead (Pb) are used as nanoparticles. Ethylene glycol ($C_2H_6O_2$) is used as a conventional liquid. Joule heating and dissipation are considered in thermal relation. Entropy generation analysis is carried out. Governing nonlinear expressions are made dimensionless by implementation of suitable transformations. ND-solve is utilized for numerical solutions. Liquid flow, entropy and temperature for both nanoliquid ($Pb/C_2H_6O_2$) and hybrid nanoliquid (Fe_2O_3 + $Pb/C_2H_6O_2$) are explored. Surface drag force and heat transport rate against emerging variables for nanoliquid ($Pb/C_2H_6O_2$) and hybrid nanoliquid (Fe_2O_3 + $Pb/C_2H_6O_2$) are numerically discussed.

2. Modeling

Two-dimensional magnetized flow of the hybrid (Fe_2O_3 + $Pb/C_2H_6O_2$) nanoliquid by the curved stretching surface is addressed. Darcy–Forchheimer model analysis is carried out. Lead (Pb) and ferric oxide (Fe_2O_3) are used as nanoparticles and ethylene glycol ($C_2H_6O_2$) as the base liquid. Cattaneo–Christov heat flux with ohmic heating and dissipation is under consideration. Entropy analysis is carried out. The surface has stretching velocity ($u_w = u_0 e^{s/L}$) with u_0 reference velocity. The magnetic field of constant strength (B_0) is applied. Fig. 1 comprises a physical model.[43]

The governing equations satisfy:[44–49]

$$\frac{\partial}{\partial r}((r+R)v) + R\frac{\partial u}{\partial s} = 0, \tag{1}$$

$$\frac{1}{(r+R)}u^2 = \frac{1}{\rho_{hnf}}\frac{\partial p}{\partial r}, \tag{2}$$

$$v\frac{\partial u}{\partial r} + \frac{uR}{(r+R)}\frac{\partial u}{\partial s} + \frac{u}{(r+R)}v = -\frac{1}{\rho_{hnf}}\frac{R}{(r+R)}\frac{\mu_{hnf}}{\rho_{hnf}}\left(\frac{\partial^2 u}{\partial r^2} + \frac{1}{(r+R)}\frac{\partial u}{\partial r} - \frac{u}{(r+R)^2}\right) - \frac{\sigma_{hnf}}{\rho_{hnf}}{B_0}^2 u - \frac{\mu_{hnf}}{\rho_{hnf}}\frac{1}{k_p}u - Fu^2\Bigg\}, \tag{3}$$

$$\left.\begin{aligned} &v\frac{\partial T}{\partial r} + \frac{uR}{(r+R)}\frac{\partial T}{\partial s} - \frac{\mu_{hnf}}{(\rho c_p)_{hnf}}\left(\frac{\partial u}{\partial r} + \frac{u}{(r+R)}\right)^2 - \frac{\sigma_{hnf}}{(\rho c_p)_{hnf}}{B_0}^2 u^2 - 2\delta_E\frac{\sigma_{hnf}}{(\rho c_p)_{hnf}}{B_0}^2\left(uv\frac{\partial u}{\partial r} + u^2\frac{R}{(r+R)}\frac{\partial u}{\partial s}\right)\\ &+\delta_E\left(\begin{aligned} &v\frac{\partial v}{\partial r}\frac{\partial T}{\partial r} + v^2\frac{\partial^2 T}{\partial r^2} + \frac{vR}{(r+R)}\frac{\partial u}{\partial r}\frac{\partial T}{\partial s} + 2uv\frac{R}{(r+R)}\frac{\partial^2 T}{\partial r\partial s} - uv\frac{R}{(r+R)^2}\frac{\partial T}{\partial s}\\ &+\frac{uR}{(r+R)}\frac{\partial T}{\partial r}\frac{\partial v}{\partial s} + u\left(\frac{R}{(r+R)}\right)^2\frac{\partial u}{\partial s}\frac{\partial T}{\partial s} + \left(\frac{uR}{(r+R)}\right)^2\frac{\partial^2 T}{\partial s^2}\end{aligned}\right)\\ &-2\delta_E\frac{\mu_{hnf}}{(\rho c_p)_{hnf}}\left(\begin{aligned} &v\frac{\partial u}{\partial r}\frac{\partial^2 u}{\partial r^2} + \frac{v}{(r+R)}\left(\frac{\partial u}{\partial r}\right)^2 + \frac{uv}{(r+R)}\frac{\partial^2 u}{\partial r^2} - \frac{u^2 v}{(r+R)^3} + \frac{uR}{(r+R)}\frac{\partial u}{\partial r}\frac{\partial^2 u}{\partial r\partial s}\\ &+\frac{u^2 R}{(r+R)^2}\frac{\partial^2 u}{\partial r\partial s} + \frac{uR}{(r+R)^2}\frac{\partial u}{\partial r}\frac{\partial u}{\partial s} + \frac{u\,R}{(r+R)^3}\frac{\partial u}{\partial s}\end{aligned}\right)\\ &=\frac{k_{hnf}}{(\rho c_p)_{hnf}}\left(\frac{\partial^2 T}{\partial r^2} + \frac{1}{r+R}\frac{\partial T}{\partial r}\right)\end{aligned}\right\}, \tag{4}$$

with[50–52]

$$\left.\begin{array}{l} u = u_w(s),\ v = 0,\ T = T_w = T_\infty + T_0 e^{\frac{As}{2L}}, \quad \text{at } r = 0 \\ u \to 0,\ T \to T_\infty, \quad \text{as } r \to \infty \end{array}\right\}. \tag{5}$$

In the above expressions (u,v) depict velocity components, μ_{hnf} the dynamic viscosity, ρ_{hnf} the density, (r,s) signify the Cartesian coordinates, σ_{hnf} the electrical conductivity, $F\left(=\frac{C_b}{\sqrt{k_p}}\right)$ the inertia coefficient, k_p the porous medium permeability coefficient, R the radius of curvature, $(\rho c_p)_{hnf}$ the heat capacitance, C_b the drag force coefficient, L the reference length, T the temperature, k_{hnf} the thermal conductivity, c_p the specific heat, T_∞ the ambient temperature, δ_E the heat relaxation time, B_0 the magnetic field strength, T_w the wall temperature and p the pressure.

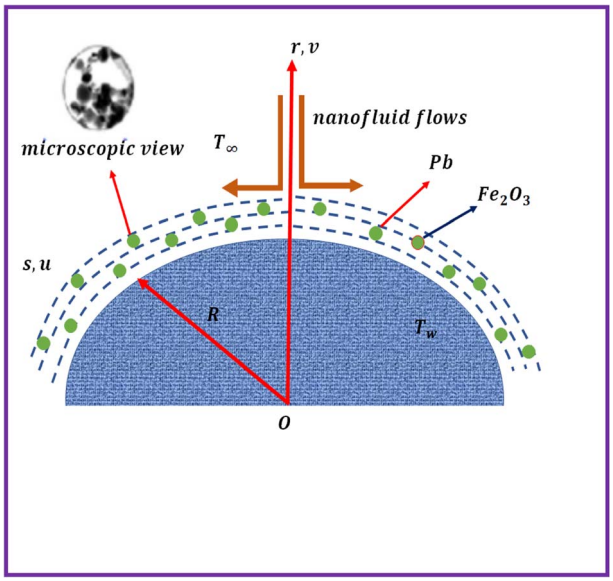

Fig. 1 Flow sketch.

2.1. Thermophysical characteristics

Mathematical expressions for nanofluid and hybrid nanomaterials and numerical values of conventional fluid and nanoparticles have been given through Tables 1 and 2.[53,54]

Letting

$$\left.\begin{array}{l} u = u_0 e^{s/L}\frac{\partial f(\xi,\eta)}{\partial \eta},\ v = -\frac{R}{r+R}\sqrt{\frac{\nu_f u_0 e^{s/L}}{2L}}\left(f(\xi,\eta) + 2\xi\frac{\partial f(\xi,\eta)}{\partial \xi} + \eta\frac{\partial f(\xi,\eta)}{\partial \eta}\right) \\ T = T_\infty + T_0 e^{\frac{As}{2L}}\theta(\xi,\eta),\ \eta = \sqrt{\frac{u_0 e^{s/L}}{2L\nu_f}}r,\ \xi = e^{s/L},\ p = \rho_f {u_0}^2 e^{\frac{2s}{L}}P(\xi,\eta) \end{array}\right\}, \tag{6}$$

one obtains

$$\frac{\partial P}{\partial \eta} = \frac{A_2}{(\eta + \sqrt{\xi}K_1)}\left(\frac{\partial f}{\partial \eta}\right)^2, \tag{7}$$

$$\left.\begin{array}{l} \left(\frac{\partial^3 f}{\partial \eta^3} + \frac{1}{(\eta+\sqrt{\xi}K_1)}\left(\frac{\partial f}{\partial \eta}\right)^2 - \frac{1}{(\eta+\sqrt{\xi}K_1)^2}\frac{\partial f}{\partial \eta}\right) - A_1\left(\frac{4\sqrt{\xi}K_1}{(\eta+\sqrt{\xi}K_1)}P(\xi,\eta) + \frac{2\sqrt{\xi}K_1}{(\eta+\sqrt{\xi}K_1)}\xi\frac{\partial P}{\partial \xi} + \frac{\sqrt{\xi}K_1}{(\eta+\sqrt{\xi}K_1)}\eta\frac{\partial P}{\partial \eta}\right) \\ +A_1A_2\left(\begin{array}{c} \frac{\sqrt{\xi}K_1}{(\eta+\sqrt{\xi}K_1)}f\frac{\partial^2 f}{\partial \eta^2} + \frac{2\sqrt{\xi}K_1}{(\eta+\sqrt{\xi}K_1)}\xi\frac{\partial f}{\partial \xi}\frac{\partial^2 f}{\partial \eta^2} - \frac{2\sqrt{\xi}K_1}{(\eta+\sqrt{\xi}K_1)}\left(\frac{\partial f}{\partial \eta}\right)^2 - \frac{2\sqrt{\xi}K_1}{(\eta+\sqrt{\xi}K_1)}\xi\frac{\partial f}{\partial \eta}\frac{\partial^2 f}{\partial \xi \partial \eta} \\ + \frac{\sqrt{\xi}K_1}{(\eta+\sqrt{\xi}K_1)^2}f\frac{\partial f}{\partial \eta} + \frac{2\sqrt{\xi}K_1}{(\eta+\sqrt{\xi}K_1)^2}\xi\frac{\partial f}{\partial \xi}\frac{\partial f}{\partial \eta} + \frac{\sqrt{\xi}K_1}{(\eta+\sqrt{\xi}K_1)^2}\eta\left(\frac{\partial f}{\partial \eta}\right)^2 \end{array}\right) \\ -A_1\frac{2}{\xi}\frac{\sigma_{hnf}}{\sigma_f}M\frac{\partial f}{\partial \eta} - \frac{2}{\xi}\lambda\frac{\partial f}{\partial \eta} - A_1A_2\mathrm{Fr}\left(\frac{\partial f}{\partial \eta}\right)^2 = 0 \end{array}\right\}, \tag{8}$$

Table 1 Mathematical expressions for thermophysical characteristics[53,54]

Properties	Nanoliquid
Viscosity	$\mu_{nf} = \frac{\mu_f}{(1-\phi_1)^{5/2}}$
Density	$\rho_{nf} = (1-\phi_1)\rho_f + \phi_1\rho_{s1}$
Heat capacity	$(\rho c_p)_{nf} = (1-\phi_1)(\rho c_p)_f + \phi_1(\rho c_p)_{s1}$
Electrical conductivity	$\frac{\sigma_{nf}}{\sigma_f} = \frac{\sigma_{s1}(1+2\phi_1) + 2\sigma_f(1-\phi_1)}{\sigma_{s1}(1-\phi_1) + \sigma_f(2+\phi_1)}$
Thermal conductivity	$\frac{k_{nf}}{k_f} = \frac{k_{s1} + 2k_f - 2\phi_1(k_f - k_{s1})}{k_{s1} + 2k_f + \phi_1(k_f - k_{s1})}$
Properties	Hybrid nanoliquid
Viscosity	$\mu_{hnf} = \frac{\mu_f}{(1-\phi_1)^{5/2}(1-\phi_2)^{5/2}}$
Density	$\rho_{hnf} = (1-\phi_2)\{(1-\phi_1)\rho_f + \phi_1\rho_{s1}\} + \phi_2\rho_{s2}$
Heat capacity	$(\rho c_p)_{hnf} = (1-\phi_2)\{(1-\phi_1)(\rho c_p)_f + \phi_1(\rho c_p)_{s1}\} + \phi_2(\rho c_p)_{s2}$
Electrical conductivity	$\frac{\sigma_{hnf}}{\sigma_{nf}} = \frac{\sigma_{s2}(1+2\phi_2) + 2\sigma_{nf}(1-\phi_2)}{\sigma_{s2}(1-\phi_2) + \sigma_{nf}(2+\phi_2)}$
Thermal conductivity	$\frac{k_{hnf}}{k_{nf}} = \frac{k_{s2} + 2k_{nf} - 2\phi_2(k_{nf} - k_{s2})}{k_{s2} + 2k_{nf} + \phi_2(k_{nf} - k_{s2})}$

Table 2 Thermophysical characteristics of ethylene glycol ($C_2H_6O_2$), lead (Pb) and ferric oxide (Fe_2O_3)[53,54]

Properties	ρ (kg m^{-3})	k (W m^{-1} K^{-1})	c_p (J k^{-1} g^{-1} K^{-1})	σ (Ω^{-1} m^{-1})
Ethylene glycol	1116.6	0.249	2382	1.07×10^{-7}
Lead (Pb)	11 343	35	130	4.55×10^{6}
Ferric oxide (Fe_2O_3)	5200	80.2	670	0.74×10^{6}

$$\left.\begin{aligned} &\frac{k_{hnf}}{k_f}\left(\frac{\partial^2\theta}{\partial\eta^2} + \frac{1}{(\eta+\sqrt{\xi}K_1)}\frac{\partial\theta}{\partial\eta}\right) + \frac{Ec}{A_1}\Pr\xi^{2-\frac{A}{L}}\left(\frac{\partial^2 f}{\partial\eta^2} + \frac{1}{(\eta+\sqrt{\xi}K_1)}\frac{\partial f}{\partial\eta}\right)^2 + \frac{\sigma_{hnf}}{\sigma_f}M\,Ec\Pr\xi^{1-\frac{A}{2}}\left(\frac{\partial f}{\partial\eta}\right)^2 \\ &+A_3\Pr\frac{\sqrt{\xi}K_1}{(\eta+\sqrt{\xi}K_1)}\left(f\frac{\partial\theta}{\partial\eta} + 2\xi\frac{\partial f}{\partial\xi}\frac{\partial\theta}{\partial\eta} - A\theta\frac{\partial f}{\partial\eta} - 2\frac{\partial f}{\partial\eta}\frac{\partial\theta}{\partial\xi}\right) + A_3\Pr\beta\left(A_{11} - \xi\left(\frac{\sqrt{\xi}K_1}{(\eta+\sqrt{\xi}K_1)}\right)^2(A_{22} - A_{33})\right) \\ &-\beta\frac{Ec}{A_1}\Pr\xi^{3-\frac{A}{2}}A_{44} - 2\frac{\sqrt{\xi}K_1}{(\eta+\sqrt{\xi}K_1)}\beta\frac{\sigma_{hnf}}{\sigma_f}M\,Ec\Pr\xi^{2-\frac{A}{2}}\left(\begin{aligned} &f\frac{\partial f}{\partial\eta}\frac{\partial^2 f}{\partial\eta^2} + 2\xi\frac{\partial f}{\partial\xi}\frac{\partial f}{\partial\eta}\frac{\partial^2 f}{\partial\eta^2} + \eta\left(\frac{\partial f}{\partial\eta}\right)^2\frac{\partial^2 f}{\partial\eta^2} \\ &-2\left(\frac{\partial f}{\partial\eta}\right)^3 - \eta\frac{\partial f}{\partial\eta}\frac{\partial^2 f}{\partial\eta^2} - 2\xi\frac{\partial f}{\partial\eta}\frac{\partial^2 f}{\partial\xi\partial\eta}\end{aligned}\right) = 0 \end{aligned}\right\}, \tag{9}$$

$$\left.\begin{aligned} &\frac{\partial f}{\partial\eta}(\xi,0) = 1, f(\xi,0) = -\xi\frac{\partial f}{\partial\xi}(\xi,0),\ \theta(\xi,0) = 1, \\ &\frac{\partial f}{\partial\eta}(\xi,\infty) = 0,\ \theta(\xi,\infty) = 0, \end{aligned}\right\}. \tag{10}$$

Here $K_1\left(=\sqrt{\frac{u_0}{2\nu_f L}}R\right)$ shows the material parameter, $Ec\left(=\frac{{u_0}^2}{c_p T_0}\right)$ the Eckert number, $Fr\left(=\frac{C_b}{\sqrt{k_p}}L\right)$ theForchheimer number, $\beta\left(=\frac{\delta_E u_0}{L}\right)$ the thermal relaxation time, $M\left(=\frac{2\sigma_f {B_0}^2 L}{u_0\rho_f}\right)$ the magnetic variable, $\Pr\left(=\frac{\nu_f}{\alpha_f}\right)$ the Prandtl number and $\lambda\left(=\frac{\nu_f L}{u_0 k_p}\right)$ the porosity parameter. Here A_1, A_2, A_3, A_{11}, A_{22}, A_{33} and A_{44} are expressed as

$$\left.\begin{aligned} A_1 &= (1-\phi_1)^{5/2}(1-\phi_2)^{5/2} \\ A_2 &= (1-\phi_2)\left((1-\phi_1) + \frac{\phi_1\rho_{s1}}{\rho_f}\right) + \frac{\phi_2\rho_{s2}}{\rho_f} \\ A_3 &= (1-\phi_2)\left((1-\phi_1) + \frac{\phi_1(\rho c_p)_{s1}}{(\rho c_p)_f}\right) + \frac{\phi_2(\rho c_p)_{s2}}{(\rho c_p)_f} \end{aligned}\right\}, \tag{11}$$

$$A_{11}=\left[\frac{1}{2}\,\xi^{2}\frac{{K_1}^{2}}{\left(\eta+\sqrt{\xi}\,K_1\right)^{3}}\left(\begin{array}{c} f^{2}\dfrac{\partial\theta}{\partial\eta}+3\xi f\,\dfrac{\partial f}{\partial\xi}\,\dfrac{\partial\theta}{\partial\eta}+2\eta f\,\dfrac{\partial f}{\partial\eta}\,\dfrac{\partial\theta}{\partial\eta}+2\xi\left(\dfrac{\partial f}{\partial\xi}\right)^{2}\dfrac{\partial\theta}{\partial\eta}\\ +\,\eta\,\dfrac{\partial f}{\partial\xi}\,\dfrac{\partial f}{\partial\eta}\,\dfrac{\partial\theta}{\partial\eta}+2\xi\eta\,\dfrac{\partial f}{\partial\xi}\,\dfrac{\partial f}{\partial\eta}\,\dfrac{\partial\theta}{\partial\eta}+\eta^{2}\left(\dfrac{\partial f}{\partial\eta}\right)^{2}\dfrac{\partial\theta}{\partial\eta}-\xi f\theta\,\dfrac{\partial f}{\partial\eta}\\ -\,2\xi^{2}A\theta\,\dfrac{\partial f}{\partial\eta}\,\dfrac{\partial f}{\partial\xi}-\xi\eta A\theta\left(\dfrac{\partial f}{\partial\eta}\right)^{2}-2\xi^{2}f\,\dfrac{\partial\theta}{\partial\xi}\,\dfrac{\partial f}{\partial\eta}\\ -\,4\xi^{2}\,\dfrac{\partial\theta}{\partial\xi}\,\dfrac{\partial f}{\partial\eta}\,\dfrac{\partial f}{\partial\xi}-2\xi^{2}\eta\,\dfrac{\partial\theta}{\partial\xi}\left(\dfrac{\partial f}{\partial\eta}\right)^{2}-\xi\eta f\,\dfrac{\partial f}{\partial\eta}\,\dfrac{\partial\theta}{\partial\eta} \end{array}\right)\right] \tag{12}$$

$$A_{22}=\left[\begin{array}{c} \dfrac{1}{2}f\,\dfrac{\partial f}{\partial\eta}\,\dfrac{\partial\theta}{\partial\eta}+\xi f\,\dfrac{\partial\theta}{\partial\eta}\,\dfrac{\partial^{2}f}{\partial\xi\partial\eta}+2\eta f\,\dfrac{\partial^{2}f}{\partial\eta^{2}}\,\dfrac{\partial\theta}{\partial\eta}+\xi\,\dfrac{\partial f}{\partial\xi}\,\dfrac{\partial f}{\partial\eta}\,\dfrac{\partial\theta}{\partial\eta}+2\xi^{2}\,\dfrac{\partial f}{\partial\xi}\,\dfrac{\partial^{2}f}{\partial\xi\partial\eta}\,\dfrac{\partial\theta}{\partial\eta}+\xi\eta\left(\dfrac{\partial f}{\partial\eta}\right)^{2}\dfrac{\partial^{2}\theta}{\partial\eta\partial\xi}\\ +\xi\eta\,\dfrac{\partial f}{\partial\xi}\,\dfrac{\partial^{2}f}{\partial\eta^{2}}\,\dfrac{\partial\theta}{\partial\eta}+\eta\left(\dfrac{\partial f}{\partial\eta}\right)^{2}\dfrac{\partial\theta}{\partial\eta}+\xi\eta\,\dfrac{\partial f}{\partial\eta}\,\dfrac{\partial\theta}{\partial\eta}+\dfrac{1}{2}\eta^{2}\,\dfrac{\partial f}{\partial\eta}\,\dfrac{\partial^{2}f}{\partial\eta^{2}}\,\dfrac{\partial\theta}{\partial\eta}+\dfrac{1}{2}f^{2}\,\dfrac{\partial^{2}\theta}{\partial\eta^{2}}+2\xi^{2}\eta\,\dfrac{\partial f}{\partial\eta}\,\dfrac{\partial\theta}{\partial\xi}\,\dfrac{\partial^{2}f}{\partial\eta\partial\xi}\\ +4\xi^{2}\left(\dfrac{\partial f}{\partial\xi}\right)^{2}\dfrac{\partial^{2}\theta}{\partial\eta^{2}}+\eta^{2}\left(\dfrac{\partial f}{\partial\eta}\right)^{2}\dfrac{\partial^{2}\theta}{\partial\eta^{2}}+4f\xi\,\dfrac{\partial f}{\partial\xi}\,\dfrac{\partial^{2}\theta}{\partial\eta^{2}}+4\xi\eta\,\dfrac{\partial f}{\partial\xi}\,\dfrac{\partial f}{\partial\eta}\,\dfrac{\partial^{2}\theta}{\partial\eta^{2}}+2\eta f\,\dfrac{\partial f}{\partial\eta}\,\dfrac{\partial^{2}\theta}{\partial\eta^{2}}+\dfrac{1}{2}A^{2}\theta\left(\dfrac{\partial f}{\partial\eta}\right)^{2}\\ +4\xi A\,\dfrac{\partial\theta}{\partial\xi}\left(\dfrac{\partial f}{\partial\eta}\right)^{2}+2\xi^{2}\,\dfrac{\partial^{2}\theta}{\partial\xi^{2}}\left(\dfrac{\partial f}{\partial\eta}\right)^{2}+\xi\eta\left(\dfrac{\partial f}{\partial\eta}\right)^{2}\dfrac{\partial^{2}\theta}{\partial\eta\partial\xi}+\dfrac{1}{2}\eta^{2}\left(\dfrac{\partial f}{\partial\eta}\right)^{2}\dfrac{\partial^{2}\theta}{\partial\eta^{2}}+\dfrac{1}{2}\eta^{2}\left(\dfrac{\partial f}{\partial\eta}\right)^{2}\dfrac{\partial^{2}\theta}{\partial\eta^{2}}\\ +\xi A^{2}\theta\,\dfrac{\partial f}{\partial\eta}\,\dfrac{\partial^{2}f}{\partial\eta\partial\xi}+2\,\dfrac{\partial\theta}{\partial\xi}\left(\dfrac{\partial f}{\partial\eta}\right)^{2}+\dfrac{1}{2}\eta A\left(\dfrac{\partial f}{\partial\eta}\right)^{2}\dfrac{\partial\theta}{\partial\eta} \end{array}\right] \tag{13}$$

$$A_{33}=\left[\left(\begin{array}{c} -\dfrac{1}{2}Af\theta\,\dfrac{\partial^{2}f}{\partial\eta^{2}}-\xi f\,\dfrac{\partial\theta}{\partial\xi}\,\dfrac{\partial^{2}f}{\partial\eta^{2}}-\dfrac{1}{2}\eta f\,\dfrac{\partial\theta}{\partial\eta}\,\dfrac{\partial^{2}f}{\partial\eta^{2}}-A\xi\theta\dfrac{\partial^{2}f}{\partial\eta^{2}}\,\dfrac{\partial f}{\partial\xi}-2\xi^{2}\,\dfrac{\partial^{2}f}{\partial\eta^{2}}\,\dfrac{\partial f}{\partial\xi}\,\dfrac{\partial\theta}{\partial\xi}\\ -\xi\eta\,\dfrac{\partial^{2}f}{\partial\eta^{2}}\,\dfrac{\partial f}{\partial\xi}\,\dfrac{\partial\theta}{\partial\eta}-\dfrac{1}{2}\eta^{2}\,\dfrac{\partial\theta}{\partial\eta}\,\dfrac{\partial f}{\partial\eta}\,\dfrac{\partial^{2}f}{\partial\eta^{2}}-2f\,\dfrac{\partial f}{\partial\eta}\,\dfrac{\partial^{2}\theta}{\partial\xi\partial\eta}-Af\,\dfrac{\partial f}{\partial\eta}\,\dfrac{\partial\theta}{\partial\eta}-f\,\dfrac{\partial f}{\partial\eta}\,\dfrac{\partial\theta}{\partial\eta}\\ -2A\xi\,\dfrac{\partial f}{\partial\eta}\,\dfrac{\partial\theta}{\partial\eta}\,\dfrac{\partial f}{\partial\xi}-5\xi\,\dfrac{\partial f}{\partial\eta}\,\dfrac{\partial\theta}{\partial\eta}\,\dfrac{\partial f}{\partial\xi}-4\xi\,\dfrac{\partial f}{\partial\eta}\,\dfrac{\partial^{2}\theta}{\partial\eta\partial\xi}\,\dfrac{\partial f}{\partial\xi}-2\xi\eta\,\dfrac{\partial f}{\partial\eta}\,\dfrac{\partial^{2}\theta}{\partial\eta^{2}}\,\dfrac{\partial f}{\partial\xi}\\ -\dfrac{5}{2}\eta\left(\dfrac{\partial f}{\partial\eta}\right)^{2}\dfrac{\partial\theta}{\partial\eta}-2\eta\left(\dfrac{\partial f}{\partial\eta}\right)^{2}\dfrac{\partial^{2}\theta}{\partial\xi\partial\eta}-\eta\left(\dfrac{\partial f}{\partial\eta}\right)^{2}\dfrac{\partial^{2}\theta}{\partial\eta^{2}}-2\xi^{2}\,\dfrac{\partial f}{\partial\eta}\,\dfrac{\partial\theta}{\partial\eta}\,\dfrac{\partial^{2}f}{\partial\xi^{2}}\\ -\eta f\,\dfrac{\partial f}{\partial\eta}\,\dfrac{\partial^{2}\theta}{\partial\eta^{2}}-\xi\eta\,\dfrac{\partial\theta}{\partial\eta}\,\dfrac{\partial f}{\partial\eta}\,\dfrac{\partial^{2}f}{\partial\eta\partial\xi}+A\theta\left(\dfrac{\partial f}{\partial\eta}\right)^{2} \end{array}\right)\right] \tag{14}$$

$$A_{44}=\left[\begin{array}{c} 2\,\dfrac{\sqrt{\xi}K_1}{\left(\eta+\sqrt{\xi}\,K_1\right)}\left(\begin{array}{c}\dfrac{1}{2}f\,\dfrac{\partial^{2}f}{\partial\eta^{2}}\,\dfrac{\partial^{3}f}{\partial\eta^{3}}+\xi\,\dfrac{\partial f}{\partial\xi}\,\dfrac{\partial^{2}f}{\partial\eta^{2}}\,\dfrac{\partial^{3}f}{\partial\eta^{3}}+\dfrac{1}{2}\,\eta\,\dfrac{\partial f}{\partial\eta}\,\dfrac{\partial^{2}f}{\partial\eta^{2}}\,\dfrac{\partial^{3}f}{\partial\eta^{3}}-\dfrac{3}{2}\,\dfrac{\partial f}{\partial\eta}\left(\dfrac{\partial^{2}f}{\partial\eta^{2}}\right)^{2}\\ -\dfrac{1}{2}\,\xi\,\dfrac{\partial f}{\partial\eta}\,\dfrac{\partial^{2}f}{\partial\eta^{2}}\,\dfrac{\partial^{3}f}{\partial\xi\partial\eta^{2}}-\dfrac{1}{2}\,\eta\,\dfrac{\partial f}{\partial\eta}\,\dfrac{\partial^{2}f}{\partial\eta^{2}}\,\dfrac{\partial^{3}f}{\partial\eta^{3}}\end{array}\right)-\dfrac{2\sqrt{\xi}K_1}{\left(\eta+\sqrt{\xi}\,K_1\right)^{3}}\left(\dfrac{\partial f}{\partial\eta}\right)^{3}\\ +\dfrac{\sqrt{\xi}K_1}{\left(\eta+\sqrt{\xi}\,K_1\right)^{2}}\left(\begin{array}{c} f+2\xi\,\dfrac{\partial f}{\partial\xi}+\eta\,\dfrac{\partial f}{\partial\eta}+f\,\dfrac{\partial f}{\partial\eta}\,\dfrac{\partial^{3}f}{\partial\eta^{3}}+2\xi\,\dfrac{\partial f}{\partial\eta}\,\dfrac{\partial f}{\partial\xi}\,\dfrac{\partial^{3}f}{\partial\eta^{3}}+\eta\,\dfrac{\partial^{3}f}{\partial\eta^{3}}\left(\dfrac{\partial f}{\partial\eta}\right)^{2}\\ -5\left(\dfrac{\partial f}{\partial\eta}\right)^{2}\dfrac{\partial^{2}f}{\partial\eta^{2}}-\xi\left(\dfrac{\partial f}{\partial\eta}\right)^{2}\dfrac{\partial^{3}f}{\partial\xi\partial\eta^{2}}-\eta\left(\dfrac{\partial f}{\partial\eta}\right)^{2}\dfrac{\partial^{3}f}{\partial\eta^{3}}-\eta\,\dfrac{\partial f}{\partial\eta}\left(\dfrac{\partial^{2}f}{\partial\eta^{2}}\right)^{2}-2\,\dfrac{\partial f}{\partial\eta}\,\dfrac{\partial^{2}f}{\partial\eta^{2}}\,\dfrac{\partial^{2}f}{\partial\xi\partial\eta}\end{array}\right)\\ +\dfrac{\sqrt{\xi}K_1}{\left(\eta+\sqrt{\xi}\,K_1\right)^{4}}\left(f\left(\dfrac{\partial f}{\partial\eta}\right)^{2}+2\xi\,\dfrac{\partial f}{\partial\xi}\,\dfrac{\partial f}{\partial\xi}+\eta\left(\dfrac{\partial f}{\partial\eta}\right)^{3}\right)-\dfrac{\sqrt{\xi}K_1}{\left(\eta+\sqrt{\xi}\,K_1\right)^{3}}\left(\eta\left(\dfrac{\partial f}{\partial\eta}\right)^{2}\dfrac{\partial^{2}f}{\partial\eta^{2}}+2\xi\left(\dfrac{\partial f}{\partial\eta}\right)^{2}\dfrac{\partial^{2}f}{\partial\xi\partial\eta}\right) \end{array}\right]. \tag{15}$$

3. Interesting quantities

3.1. Surface drag force

One may write

$$C_{f,s} = \frac{\tau_{rs}|_{r=0}}{\rho_f {u_w}^2}. \tag{16}$$

Here τ_{rs} wall shear stress is

$$\tau_{rs} = \mu_{hnf}\left(\frac{\partial u}{\partial r} - \frac{1}{(r+R)}u\right), \tag{17}$$

Dimensionless version is

$$C_{fs}{\mathrm{Re}_s}^{1/2} = \frac{1}{A_1}\left(f''(0) + \frac{1}{K_1}f'(0)\right). \tag{18}$$

3.2. Nusselt number

Considering

$$\mathrm{Nu}_s = \frac{sq_w}{k_f(T_w - T_\infty)}, \tag{19}$$

and heat flux q_w

$$q_w = -k_{hnf}\left(\frac{\partial T}{\partial r}\right)\Big|_{r=0}, \tag{20}$$

we can express that

$$\sqrt{\frac{2L}{s}}\mathrm{Nu}_s{\mathrm{Re}_s}^{-1/2} = -\frac{k_{hnf}}{k_f}\theta'(0), \tag{21}$$

in which $\mathrm{Re}_s = \frac{u_w s}{\nu_f}$ indicates the local Reynolds number.

4. Entropy formulation

Mathematical expression is given by

$$E_G(\xi,\eta) = \frac{1}{{T_\infty}^2}k_{hnf}\left(\frac{\partial T}{\partial r}\right)^2 + \frac{\mu_{hnf}}{T_\infty}\left(\frac{\partial u}{\partial r} + \frac{u}{r+R}\right)^2 + \frac{\mu_{hnf}}{T_\infty}\frac{1}{k_p}u^2 + \frac{\sigma_{hnf}}{T_\infty}{B_0}^2u^2, \tag{22}$$

or

$$S_G(\xi,\eta) = \alpha_1\frac{k_{hnf}}{k_f}\xi^{(1+A)}\left(\frac{\partial\theta}{\partial\eta}\right)^2 + \frac{1}{A_1}\mathrm{Br}\xi^3\left(\frac{\partial^2 f}{\partial\eta^2} + \frac{1}{(\eta+\sqrt{\xi}K_1)}\frac{\partial f}{\partial\eta}\right)^2 + \frac{1}{A_1}\lambda\mathrm{Br}\xi^2\left(\frac{\partial f}{\partial\eta}\right)^2 + \frac{\sigma_{hnf}}{\sigma_f}M\mathrm{Br}\xi^2\left(\frac{\partial f}{\partial\eta}\right)^2\Bigg\}. \tag{23}$$

Here $\alpha_1\left(=\frac{T_0}{T_\infty}\right)$ represents the heat ratio parameter, $\mathrm{Br}\left(=\frac{\mu_f {u_0}^2}{T_0 k_f}\right)$ the Brinkman number and $S_G\left(=\frac{2E_G L T_\infty \nu_f}{k_f u_0 T_0}\right)$ the entropy rate.

5. Solutions methodology

Considering the derivatives with respect to ξ $\left(i.e.\ \frac{\partial(\cdot)}{\partial\xi} = 0\right)$ in eqn (7)–(10) we arrive at

$$P' = \frac{A_2}{(\eta+\sqrt{\xi}K_1)}{f'}^2, \tag{24}$$

$$\left.\begin{aligned}&\left(f''' + \frac{1}{(\eta+\sqrt{\xi}K_1)}{f'}^2 - \frac{1}{(\eta+\sqrt{\xi}K_1)^2}f'\right) - A_1\left(\frac{4\sqrt{\xi}K_1}{(\eta+\sqrt{\xi}K_1)}P + \frac{\sqrt{\xi}K_1}{(\eta+\sqrt{\xi}K_1)}\eta P'\right)\\ &+A_1A_2\left(\frac{\sqrt{\xi}K_1}{(\eta+\sqrt{\xi}K_1)}ff'' - \frac{2\sqrt{\xi}K_1}{(\eta+\sqrt{\xi}K_1)}{f'}^2 + \frac{\sqrt{\xi}K_1}{(\eta+\sqrt{\xi}K_1)^2}ff' + \frac{\sqrt{\xi}K_1}{(\eta+\sqrt{\xi}K_1)^2}\eta{f'}^2\right)\\ &-A_1\frac{2}{\xi}\frac{\sigma_{hnf}}{\sigma_f}Mf' - \frac{2}{\xi}\lambda f' - A_1A_2\mathrm{Fr}{f'}^2 = 0\end{aligned}\right\}, \tag{25}$$

$$\left.\begin{aligned}&\frac{k_{hnf}}{k_f}\left(\theta'' + \frac{1}{(\eta+\sqrt{\xi}K_1)}\theta'\right) + \frac{\mathrm{Ec}}{A_1}\mathrm{Pr}\xi^{2-\frac{A}{2}}\left(f'' + \frac{1}{(\eta+\sqrt{\xi}K_1)}f'\right)^2 + \frac{\sigma_{hnf}}{\sigma_f}M\mathrm{Ec}\mathrm{Pr}\xi^{1-\frac{A}{2}}{f'}^2\\ &+A_3\mathrm{Pr}\frac{\sqrt{\xi}K_1}{(\eta+\sqrt{\xi}K_1)}\left(f\theta' - A\theta f'\right) + A_3\mathrm{Pr}\beta A_{55} - \beta\frac{\mathrm{Ec}}{A_1}\mathrm{Pr}\xi^{3-\frac{A}{2}}A_{66}\\ &-2\frac{\sqrt{\xi}K_1}{(\eta+\sqrt{\xi}K_1)}\frac{\sigma_{hnf}}{\sigma_f}\beta M\mathrm{Ec}\mathrm{Pr}\xi^{2-\frac{A}{2}}\left(ff'f'' + \eta{f'}^2f'' - 2{f'}^3 - \eta f'f''\right) = 0\end{aligned}\right\}, \tag{26}$$

$$\left.\begin{array}{c} f'(\xi,0)=1,\ f(\xi,0)=0,\ \theta(\xi,0)=1, \\ f'(\xi,\infty)=0,\ \theta(\xi,\infty)=0 \end{array}\right\} \tag{27}$$

with A_{55} and A_{66} as

$$A_{55}=\begin{bmatrix} \frac{1}{2}\xi^2\frac{{K_1}^2}{\left(\eta+\sqrt{\xi}K_1\right)^3}\left(f^2\theta'+2\eta f'\theta'+\eta^2 f'^2\theta'-\xi f\theta f'-\xi\eta A\theta f'^2-\xi\eta f f'\theta'\right) \\ -\xi\left(\frac{\sqrt{\xi}K_1}{\left(\eta+\sqrt{\xi}K_1\right)}\right)^2\begin{pmatrix} \frac{1}{2}ff'\theta'+2\eta ff''\theta'-\frac{3}{2}\eta f'^2\theta'+\xi\eta f'\theta'+\frac{1}{2}f^2\theta'' \\ +\eta^2 f'^2\theta''+2\eta ff'\theta''-\frac{1}{2}Af\theta f''-\frac{1}{2}\eta f\theta' f''-Aff'\theta'-ff'\theta' \\ -\eta ff'\theta''+\frac{1}{2}\eta Af'^2\theta'-\eta f'^2\theta''+\frac{1}{2}A^2\theta f'^2+\frac{1}{2}\eta^2 f'^2\theta''+A\theta f'^2 \end{pmatrix} \end{bmatrix} \tag{28}$$

$$A_{66}=\begin{bmatrix} \frac{\sqrt{\xi}K_1}{\left(\eta+\sqrt{\xi}K_1\right)^2}\left(f+\eta f'+ff'f'''+\eta f'''f'^2-5f'^2f''-\eta f'^2f'''-\eta f'f''^2\right) \\ +2\frac{\sqrt{\xi}K_1}{\left(\eta+\sqrt{\xi}K_1\right)}\left(\frac{1}{2}ff''f'''-\frac{3}{2}f'f''^2\right)+\frac{\sqrt{\xi}K_1}{\left(\eta+\sqrt{\xi}K_1\right)^4}\left(ff'^2+\eta f'^3\right)-\frac{\sqrt{\xi}K_1}{\left(\eta+\sqrt{\xi}K_1\right)^3}\left(2f'^3+\eta f'^2f''\right) \end{bmatrix} \tag{29}$$

Elimination of pressure from eqn (22) and (23) yields

$$\left.\begin{array}{c} \frac{1}{A_1}\left(f^{(\mathrm{iv})}+\frac{2}{\left(\eta+\sqrt{\xi}K_1\right)}f'''-\frac{1}{\left(\eta+\sqrt{\xi}K_1\right)^2}f''+\frac{1}{\left(\eta+\sqrt{\xi}K_1\right)^3}f'-2\frac{\lambda}{\xi}\left(f''+\frac{1}{\left(\eta+\sqrt{\xi}K_1\right)}f'\right)\right) \\ +A_2\frac{\sqrt{\xi}K_1}{\left(\eta+\sqrt{\xi}K_1\right)}\begin{pmatrix} ff'''-\frac{1}{\left(\eta+\sqrt{\xi}K_1\right)^2}ff'+\frac{1}{\left(\eta+\sqrt{\xi}K_1\right)}ff''-\frac{2\sqrt{\xi}K_1}{\left(\eta+\sqrt{\xi}K_1\right)}f'^2-3f'f'' \\ +\frac{2}{\left(\eta+\sqrt{\xi}K_1\right)}(\eta-1)f'f'''-\frac{1}{\left(\eta+\sqrt{\xi}K_1\right)}(1+2\eta)f'^2 \end{pmatrix} \\ -\frac{2}{\xi}\frac{\sigma_{\mathrm{hnf}}}{\sigma_{\mathrm{f}}}M\left(f''+\frac{1}{\left(\eta+\sqrt{\xi}K_1\right)}f'\right)-2A_2\mathrm{Fr}\left(2f'f''+\frac{1}{\left(\eta+\sqrt{\xi}K_1\right)}f'^2\right)=0 \end{array}\right\}. \tag{30}$$

5.1. Numerical approach

Governing problems are solved by the ND-solve algorithm. The Mathematica software is utilized to develop the computational results. For this we converted the boundary value problem to the initial value situation as follows:

$$\left.\begin{array}{c} f=y_1,\ f'=y_2,\ f''=y_3,\ f'''=y_4,\ f^{\mathrm{iv}}=y'_4 \\ \theta=y_5,\ \theta'=y_6,\ \theta''=y'_6 \end{array}\right\}, \tag{31}$$

$$y'_4 = \left\{ \begin{array}{c} \frac{1}{(\eta+\sqrt{\xi}\,K_1)^2}y_3 - \frac{2}{(\eta+\sqrt{\xi}\,K_1)}y_4 - \frac{1}{(\eta+\sqrt{\xi}\,K_1)^3}y_2 + \frac{2\lambda}{\xi}\left(y_3 + \frac{1}{(\eta+\sqrt{\xi}\,K_1)}y_2\right) \\ -A_1A_2\frac{\sqrt{\xi}K_1}{(\eta+\sqrt{\xi}\,K_1)}\left(\begin{array}{c} y_1y_4 - \frac{1}{(\eta+\sqrt{\xi}\,K_1)}y_1y_2 + \frac{1}{(\eta+\sqrt{\xi}\,K_1)}y_1y_3 - \frac{2\sqrt{\xi}K_1}{(\eta+\sqrt{\xi}\,K_1)}{y_2}^2 \\ -3y_2y_3 + \frac{2}{(\eta+\sqrt{\xi}\,K_1)}(\eta-1)y_1y_3 - \frac{1}{(\eta+\sqrt{\xi}\,K_1)}(1+2\eta){y_2}^2 \end{array}\right) \\ +\frac{2}{\xi}A_1\frac{\sigma_{\mathrm{hnf}}}{\sigma_{\mathrm{f}}}M\left(y_3 - \frac{1}{(\eta+\sqrt{\xi}\,K_1)}y_2\right) - 2A_1A_2\mathrm{Fr}\left(2y_1y_3 + \frac{1}{(\eta+\sqrt{\xi}\,K_1)}{y_2}^2\right) \end{array} \right\} \tag{32}$$

$$y'_6 = \left\{ \begin{array}{c} -\frac{1}{(\eta+\sqrt{\xi}\,K_1)} - \frac{k_{\mathrm{f}}}{k_{\mathrm{hnf}}}\left(\frac{\mathrm{PrEc}}{A_1}\xi^{2-\frac{A}{2}}\left(y_3 + \frac{1}{(\eta+\sqrt{\xi}\,K_1)}y_2\right)^2 + \frac{\sigma_{\mathrm{hnf}}}{\sigma_{\mathrm{f}}}M\mathrm{PrEc}\xi^{1-\frac{A}{2}}{y_2}^2\right) \\ -\frac{k_{\mathrm{f}}}{k_{\mathrm{hnf}}}A_3\mathrm{Pr}\frac{\sqrt{\xi}K_1}{(\eta+\sqrt{\xi}\,K_1)}(y_1y_6 - Ay_2y_5) - \frac{k_{\mathrm{f}}}{k_{\mathrm{hnf}}}\left(A_3\mathrm{Pr}\beta A_{77} - \frac{\beta\mathrm{PrEc}}{A_1}\xi^{3-\frac{A}{2}}A_{88}\right) \\ +\frac{2\sqrt{\xi}K_1}{(\eta+\sqrt{\xi}\,K_1)}\frac{k_{\mathrm{f}}}{k_{\mathrm{hnf}}}\frac{\sigma_{\mathrm{hnf}}}{\sigma_{\mathrm{f}}}M\mathrm{PrEc}\xi^{2-\frac{A}{2}}(y_1y_2y_3 - \eta{y_2}^2y_3 - 2{y_2}^3 - \eta y_2y_3) \end{array} \right\} \tag{33}$$

$$\left.\begin{array}{c} y_1(0) = 0,\ y_2(0) = 1,\ y_5(0) = 0 \\ y_2(\infty) = 0,\ y_5(\infty) = 0 \end{array}\right\} \tag{34}$$

with A_{77} and A_{88} given below:

$$A_{77} = \left\{ \begin{array}{c} \frac{\xi^2{K_1}^2}{2(\eta+\sqrt{\xi}\,K_1)}({y_1}^2y_6 + 2\eta y_2y_6 + \eta^2{y_2}^2y_6 - \xi y_1y_2y_5 - \xi\eta{y_2}^2y_5 - \xi\eta y_1y_2y_6) \\ -\xi\left(\frac{\sqrt{\xi}K_1}{(\eta+\sqrt{\xi}\,K_1)}\right)^2\left(\frac{1}{2}\,y_1y_2y_5 + 2\eta y_1y_3y_5 - \frac{3}{2}\,\eta{y_2}^2y_5 + \xi\eta y_2y_5 + \frac{1}{2}\,\eta{y_1}^2y'_6 + \eta^2{y_2}^2y'_6\right) \\ -\xi\left(\frac{\sqrt{\xi}K_1}{(\eta+\sqrt{\xi}\,K_1)}\right)^2\left(-\frac{1}{2}\,Ay_1y_3y_5 - \frac{1}{2}\,\eta y_1y_3y_6 - Ay_1y_2y_5 - y_1y_2y_6 - \eta y_1y_2y'_6 + \frac{1}{2}\,A{y_2}^2y_6\right) \\ -\xi\left(\frac{\sqrt{\xi}K_1}{(\eta+\sqrt{\xi}\,K_1)}\right)^2\left(\eta{y_2}^2y_6 + \frac{1}{2}\,A^2{y_2}^2y_5 + \frac{1}{2}\,\eta^2{y_2}^2y'_6 + A{y_2}^2y_5\right) \end{array} \right\} \tag{35}$$

$$A_{88} = \left\{ \begin{array}{c} \frac{\sqrt{\xi}K_1}{(\eta+\sqrt{\xi}\,K_1)^2}({y_1} + \eta y_2 + y_1y_2y_4 + \eta{y_2}^2y_4 - 5{y_2}^2y_3 - \eta{y_1}^2y_4 - \eta y_2{y_3}^2) \\ +\frac{\sqrt{\xi}K_1}{(\eta+\sqrt{\xi}\,K_1)}({y_1}y_3y_4 - 3y_2{y_3}^2 + y_1{y_2}^2 + \eta{y_2}^3 - 2{y_2}^3 - \eta{y_2}^2y_3) \end{array} \right\} \tag{36}$$

6. Discussion

The influence of emerging variables on liquid flow, entropy rate and temperature for both nanoliquid ($Pb/C_2H_6O_2$) and hybrid nanoliquid ($Fe_2O_3 + Pb/C_2H_6O_2$) is discussed. Here dotted lines show nanoliquid ($Pb/C_2H_6O_2$) behaviors and solid lines characterize the hybrid ($Pb + Fe_2O_3/C_2H_6O_2$) nanoliquid characteristics. Engineering quantities like the skin friction coefficient and heat transport rate are discussed through tabulated forms. Comparison of recent analysis with previous results in the literature is constructed in Table 3. Here we discussed the

Table 3 Coefficient of skin friction comparison with Okechi *et al.*[55]

K_1	Okechi *et al.*[55]	Present results
5	1.4196	1.41963
10	1.3467	1.34675
20	1.3135	1.31354
30	1.3028	1.30281

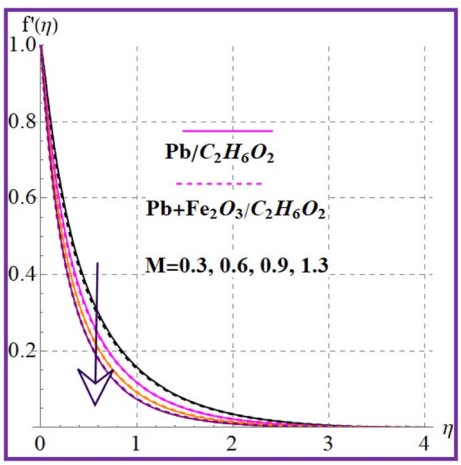

Fig. 2 $f'(\eta)$ variation *versus* M.

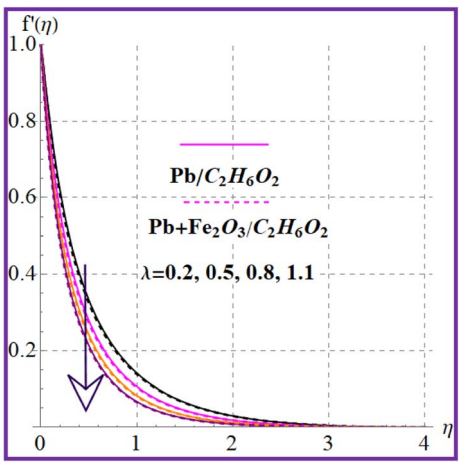

Fig. 3 $f'(\eta)$ variation *versus* λ.

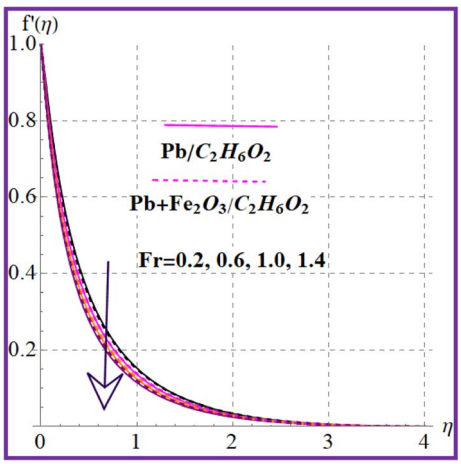

Fig. 4 $f'(\eta)$ variation *versus* Fr.

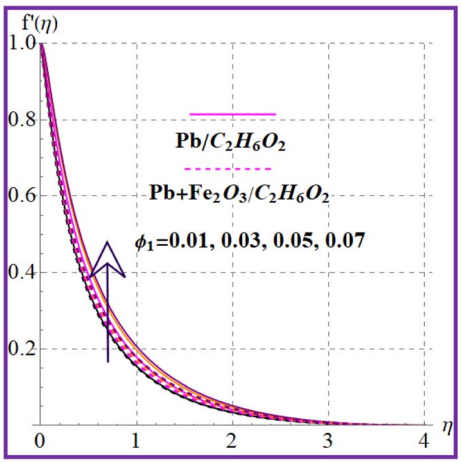

Fig. 5 $f'(\eta)$ variation *versus* ϕ_1.

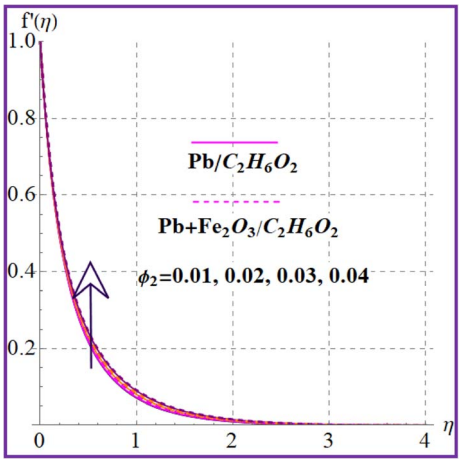

Fig. 6 $f'(\eta)$ variation *versus* ϕ_2.

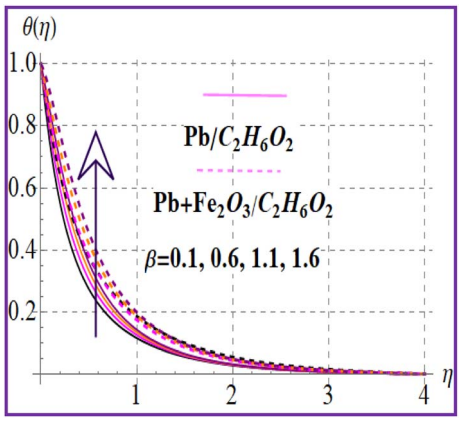

Fig. 7 $\theta(\eta)$ *versus* β.

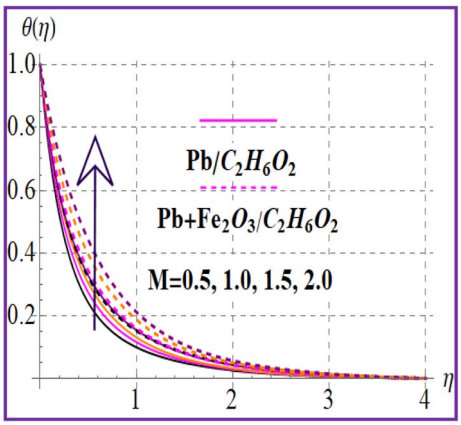

Fig. 8 $\theta(\eta)$ *versus* M.

comparison of the coefficient of skin friction *versus* a higher approximation of the curvature variable with Okechi *et al.*[55] for a limiting case (viscous fluid flow). Clearly a good consensus is noticed.

6.1. Velocity

Fig. 2 illustrates the flow behavior against the magnetic variable (M). An increment in the magnetic variable leads to

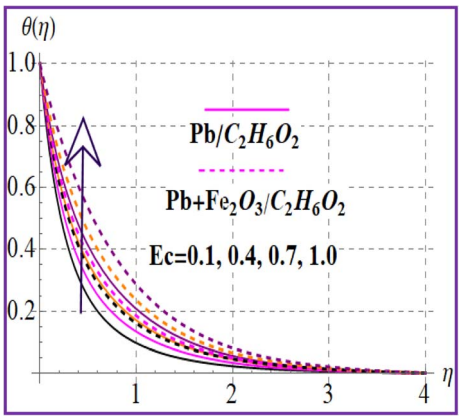

Fig. 9 $\theta(\eta)$ *versus* Ec.

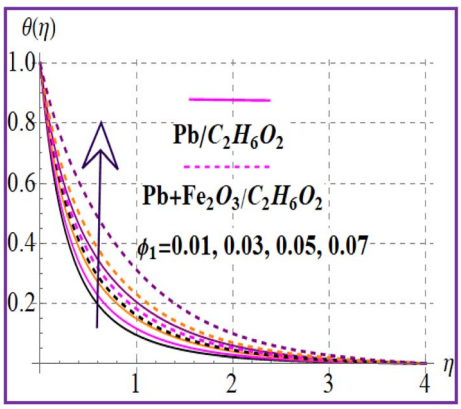

Fig. 10 $\theta(\eta)$ *versus* ϕ_1.

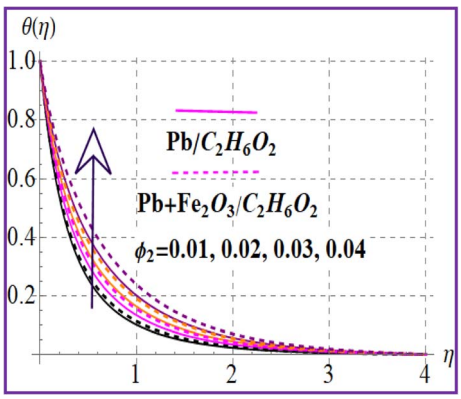

Fig. 11 $\theta(\eta)$ *versus* ϕ_2.

intensification of the Lorentz force which declines the liquid flow. The influence of (λ) on ($f'(\eta)$) is portrayed in Fig. 3. Higher porosity corresponds to diminished velocity in both nanoliquid ($Pb/C_2H_6O_2$) and hybrid ($Pb + Fe_2O_3/C_2H_6O_2$) nanoliquid cases. Fig. 4 shows the velocity impact against the Forchheimer number (Fr). A reduction in liquid flow ($f'(\eta)$) is noticed *versus* the Forchheimer number for both nanoliquid ($Pb/C_2H_6O_2$) and hybrid ($Pb + Fe_2O_3/C_2H_6O_2$) nanomaterials. Fig. 5 and 6

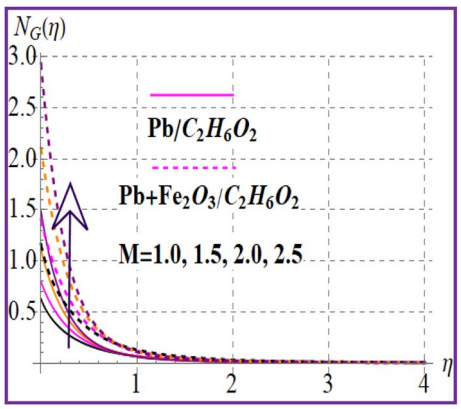

Fig. 12 $N_G(\eta)$ *versus* M.

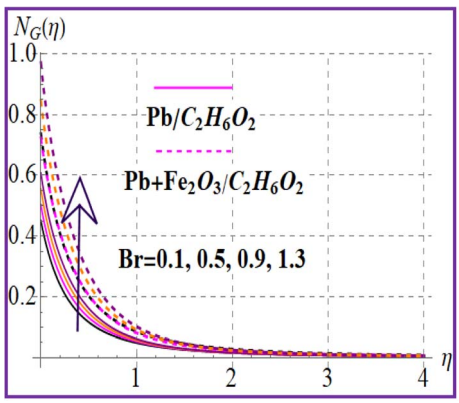

Fig. 13 $N_G(\eta)$ *versus* Br.

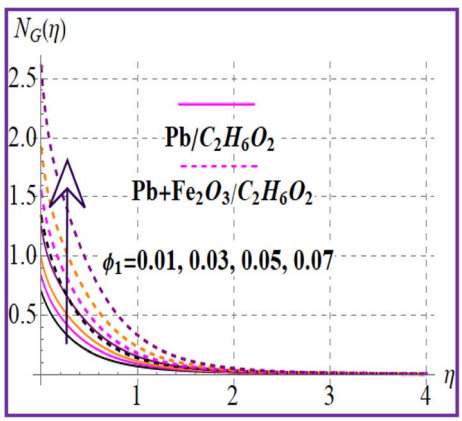

Fig. 14 $N_G(\eta)$ *versus* ϕ_1.

elucidate the impact for flow *versus* nanoparticle volume fractions (ϕ_1 and ϕ_2). It is noticed that there is an enhancement in liquid flow *versus* higher nanoparticle volume fractions (ϕ_1 and ϕ_2).

6.2. Thermal field

Fig. 7 presents the trend of temperature against the thermal relaxation time variable (β). A higher estimation of thermal relaxation time corresponds to an increase of the thermal field. Fig. 8 indicates the importance for (M) on $\theta(\eta)$. A larger approximation of the magnetic variable intensifies the Lorentz force which raises the resistance to flow. Therefore, the temperature is increased. The influence of the Eckert number on ($\theta(\eta)$) is depicted in Fig. 9. The outcome for the Eckert number (Ec) leads to creation of an additional kinetic energy and consequently the thermal field is improved. Characteristics of nanoparticle volume fractions (ϕ_1 and ϕ_2) on the thermal field are disclosed in Fig. 10 and 11. Clearly, higher nanoparticle volume fractions (ϕ_1 and ϕ_2) enhance the thermal field for both nanoliquid ($Pb/C_2H_6O_2$) and hybrid ($Pb + Fe_2O_3/C_2H_6O_2$) nanomaterials.

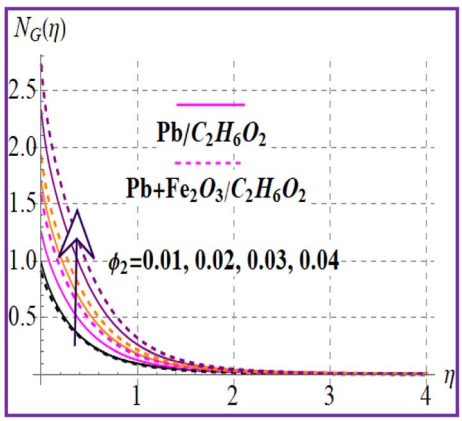

Fig. 15 $N_G(\eta)$ *versus* ϕ_2.

Table 4 Numerical results of the skin friction ($Re_s^{1/2}C_{fs}$) coefficient

				$Re_s^{1/2}C_{fs}$	
M	K_1	λ	Fr	$Pb/C_2H_6O_2$	Pb + $Fe_2O_3/C_2H_6O_2$
0.4	0.1	0.1	0.2	8.4631	19.9922
0.8				7.35445	17.5033
0.12				6.57457	15.7212
0.3	0.45	0.1	0.2	0.475582	1.04693
	0.45			0.34613	0.754253
	0.51			0.231708	0.496568
0.3	0.45	0.2	0.2	0.344601	0.738767
		0.3		0.223838	0.453805
		0.4		0.11172	0.188597
			0.1	0.564833	1.20704
			0.4	0.313042	0.748393
			0.7	0.0991132	0.343877

Table 5 Computational values for $Re_s^{-1/2}Nu_s$

				$Re_s^{-1/2}Nu_s$	
β	M	Pr	Ec	$Pb/C_2H_6O_2$	Pb + $Fe_2O_3/C_2H_6O_2$
0.01	0.1	5.0	0.4	2.94351	3.10761
0.03				2.81501	2.44288
0.05				2.68726	2.09427
0.01	0.4	5.0	0.4	2.59787	2.34593
			0.5	2.48648	1.82663
			0.6	2.37692	1.59412
0.01	0.1	3.5	0.4	2.45597	2.38122
		4.0		2.62835	2.52681
		4.5		2.79038	2.6638
0.01	0.1	5.0	0.2	3.23399	3.85736
			0.7	2.50778	1.71628
			0.11	1.92682	0.280292

6.3. Entropy rate

Fig. 12 reveals the impact of the magnetic variable on $N_G(\eta)$. Increasing values of the magnetic variable enhance the resistive force in the flow region which produces an additional energy in the system and therefore entropy is maximized. Fig. 13 depicts the importance of entropy for the Brinkman number. The

entropy rate rises *versus* a higher Brinkman number due to the viscous force. Fig. 14 and 15 show entropy characteristics against nanoparticle volume fractions (ϕ_1 and ϕ_2). A higher estimation of volume fractions (ϕ_1 and ϕ_2) leads to augmentation of the entropy rate for both nanoliquid ($Pb/C_2H_6O_2$) and hybrid ($Pb + Fe_2O_3/C_2H_6O_2$) nanomaterials.

6.4. Physical quantities

Engineering quantities like the skin friction coefficient ($Re_s^{1/2}C_{fs}$) and heat transport rate ($Re_s^{-1/2}Nu_s$) for nanoliquid ($Pb/C_2H_6O_2$) and hybrid ($Pb + Fe_2O_3/C_2H_6O_2$) nanomaterials are discussed through tabulated forms.

6.4.1. Skin friction. Table 4 highlights the characteristics of the skin friction ($Re_s^{1/2}C_{fs}$) coefficient against sundry parameters for both nanoliquid ($Pb/C_2H_6O_2$) and hybrid ($Pb + Fe_2O_3/C_2H_6O_2$) nanomaterials. It is found that larger Forchheimer number (Fr), porosity (λ), material (K_1) and magnetic (M) parameters result in skin friction reduction.

6.4.2. Heat transport rate. Table 5 shows the heat transport rate ($Re_s^{-1/2}Nu_s$) variation *versus* influential variables for both nanoliquid ($Pb/C_2H_6O_2$) and hybrid ($Pb + Fe_2O_3/C_2H_6O_2$) nanomaterials. Decay in the thermal transport rate is witnessed for larger Eckert number (Ec), thermal relaxation time (β) and magnetic (M) variables. An increment in the temperature gradient is detected for the Prandtl number.

7. Closing remarks

Main findings are listed below.

- A higher magnetic parameter decays fluid flow whereas temperature enhances.
- Velocity for the Forchheimer number and porosity parameter is the same.
- A larger thermal relaxation time variable raises temperature.
- A larger estimation of nanoparticle volume fractions corresponds to an amplified fluid flow and thermal field.
- Entropy shows increasing behavior due to the Brinkman number.
- A Higher magnetic parameter leads to entropy rate enhancement.
- Surface drag force shows decreasing behavior for Forchheimer, porosity, material and magnetic parameters.
- The Prandtl number leads to Nusselt number enhancement.
- Nusselt number improvement against thermal relaxation time and magnetic parameters is ensured.

Conflicts of interest

There are no conflicts to declare.

References

1 S. U. S. Choi and J. A. Eastman, Enhancing thermal conductivity of fluids with nanoparticles, *ASME International Mechanical Engineering Congress and Exposition*, San Francisco, California, vol. 231, 1995, pp. 99–105.
2 J. A. Eastman, S. U. S. Choi, S. Li, W. Yu and L. J. Thompson, Anomalously increased effective thermal conductivities of ethylene glycol-based nanofluids containing copper nanoparticles, *Appl. Phys. Lett.*, 2001, **78**, 718–720.
3 A. Hassan, N. Alsubaie, F. M. Alharbi, A. Alhushaybari and A. M. Galal, Scrutinization of Stefan suction/blowing on thermal slip flow of ethylene glycol/water based hybrid ferro-fluid with nano-particles shape effect and partial slip, *J. Magn. Magn. Mater.*, 2023, **565**, 170276.
4 I. Chabani, F. M. Oudina, H. Vaidya and A. I. Ismail, Numerical analysis of magnetic hybrid nano-fluid natural convective flow in an adjusted porous trapezoidal enclosure, *J. Magn. Magn. Mater.*, 2022, **564**, 170142.
5 S. A. Abdollahi, A. Alizadeh, I. C. Esfahani, M. Zarinfar and P. Pasha, Investigating heat transfer and fluid flow betwixt parallel surfaces under the influence of hybrid nanofluid suction and injection with numerical analytical technique, *Alexandria Eng. J.*, 2023, **70**, 423–439.
6 K. Alqawasmi, K. A. M. Alharbi, U. Farooq, S. Noreen, M. Imran, A. Akgül, M. Kanan and J. Asad, Numerical approach toward ternary hybrid nanofluid flow with nonlinear heat source-sink and Fourier heat flux model passing through a disk, *Int. J. Thermofluids*, 2023, **18**, 100367.
7 H. Maiti, A. Y. Khan, S. Mondal and S. K. Nandy, Scrutinization of unsteady MHD fluid flow and entropy generation: hybrid nanofluid model, *Journal of Computational Mathematics and Data Science*, 2023, **6**, 100074.
8 A. Rauf, F. Hussain, A. Mushtaq, N. A. Shah and M. R. Ali, MHD mixed convection flow for Maxwell hybrid nanofluid with Soret, Dufour and morphology effects, *Arabian J. Chem.*, 2023, **16**, 104965.
9 S. Qayyum, Dynamics of Marangoni convection in hybrid nanofluid flow submerged in ethylene glycol and water base fluids, *Int. Commun. Heat Mass Transfer*, 2020, **119**, 104962.
10 A. Y. Sayed, S. I. Ahmed, K. S. Mekheimer and M. S. Abdelwahed, Electromagnetohydrodynamic effects with single-walled carbon nanotubes particles in a corrugated microchannel, *Chaos, Solitons Fractals*, 2023, **168**, 113126.
11 S. S. Ghadikolaei and M. Gholinia, Terrific effect of H_2 on 3D free convection MHD flow of $C_2H_6O_2$ single bond H_2O hybrid base fluid to dissolve Cu nanoparticles in a porous space considering the thermal radiation and nanoparticle shapes effects, *Int. J. Hydrogen Energy*, 2019, **44**, 17072–17083.
12 T. Salahuddin, M. Khan, S. Sakinder and B. A. Alwan, A flow analysis of hybrid nanoparticles near a solid sphere, *Int. J. Hydrogen Energy*, 2022, **47**, 16640–16648.
13 A. Ali, S. Sarkar, S. Das and R. N. Jana, Investigation of Cattaneo–Christov double diffusions theory in bioconvective slip flow of radiated magneto-cross-nanomaterial over stretching cylinder/plate with activation energy, *Int. J. Appl. Comput. Math.*, 2021, **7**, 208.

14 M. V. Krishna, N. A. Ahammad and A. J. Chamkha, Radiative MHD flow of Casson hybrid nanofluid over an infinite exponentially accelerated vertical porous surface, *Case Stud. Therm. Eng.*, 2021, **27**, 101229.
15 P. Sreedevi, P. S. Reddy and A. J. Chamkha, Heat and mass transfer analysis of unsteady hybrid nanofluid flow over a stretching sheet with thermal radiation, *SN Appl. Sci.*, 2020, **2**, 1222.
16 J. B. J. Fourier, *Théorie Analytique De La Chaleur*, 1822.
17 C. Cattaneo, Sulla conduzione del calore, *Atti Semin, Mat Fis Univ Modena Reggio Emilia*, 1948, vol. 3, pp. 83–101.
18 C. I. Christov, On frame indifferent formulation of the Maxwell-Cattaneo model of finite-speed heat conduction, *Mech. Res. Commun.*, 2009, **36**, 481–486.
19 A. Razaq, S. A. Khan, T. Hayat and A. Alsaedi, Entropy optimization in radiative flow of Reiner-Rivlin material with heat source and modified Cattaneo-Christov heat and mass fluxes, *Case Stud. Therm. Eng.*, 2023, **45**, 102985.
20 A. Salmi, H. A. Madkhali, B. Ali, M. Nawaz, S. O. Alharbi and A. S. Alqahtani, Numerical study of heat and mass transfer enhancement in Prandtl fluid MHD flow using Cattaneo-Christov heat flux theory, *Case Stud. Therm. Eng.*, 2022, **33**, 101949.
21 M. Haneef, M. Nawaz, S. O. Alharbi and Y. Elmasry, Cattaneo-Christov heat flux theory and thermal enhancement in hybrid nano Oldroyd-B rheological fluid in the presence of mass transfer, *Int. Commun. Heat Mass Transfer*, 2021, **126**, 105344.
22 T. Hayat, S. A. Khan, M. I. Khan, S. Momani and A. Alsaedi, Cattaneo-Christov (CC) heat flux model for nanomaterial stagnation point flow of Oldroyd-B fluid, *Comput. Methods Programs Biomed.*, 2020, **187**, 105247.
23 S. A. Lone, S. Anwar, Z. Raizah, M. Y. Almusawa and A. Saeed, A magnetized Maxwell nanofluid flow over a stratified stretching surface with Cattaneo-Christov double diffusion theory, *J. Magn. Magn. Mater.*, 2023, **575**, 170722.
24 A. Alsaedi, S. A. Khan and T. Hayat, Cattaneo-Christov double diffusive and model development for entropy optimized flow of Reiner-Rivlin material in thermal system and environmental effect, *Alexandria Eng. J.*, 2023, **72**, 67–82.
25 S. Bilal, M. I. Shah, N. Z. Khan, A. Akgül and K. S. Nisar, Onset about non-isothermal flow of Williamson liquid over exponential surface by computing numerical simulation in perspective of Cattaneo Christov heat flux theory, *Alexandria Eng. J.*, 2022, **61**, 6139–6150.
26 M. Yasir, M. Khan, A. S. Alqahtani and M. Y. Malik, Heat generation/absorption effects in thermally radiative mixed convective flow of Zn−TiO2/H2O hybrid nanofluid, *Case Stud. Therm. Eng.*, 2023, **45**, 103000.
27 T. Salahuddin, M. Awais, M. Khan and M. Altanji, Analysis of transport phenomenon in cross fluid using Cattaneo-Christov theory for heat and mass fluxes with variable viscosity, *Int. Commun. Heat Mass Transfer*, 2021, **129**, 105664.
28 S. A. Khan, T. Hayat and A. Alsaedi, Cattaneo Christov (CC) heat and mass fluxes in Stagnation point flow of Jeffrey nanoliquids by a stretched surface, *Chin. J. Phys.*, 2022, **76**, 205–216.
29 A. Bejan, A study of entropy generation in fundamental convective heat transfer, *ASME J. Heat Mass Transfer*, 1979, **101**, 718–725.
30 A. Bejan, Entropy generation through heat and fluid flow, *J. Appl. Mech.*, 1983, **50**, 475.
31 A. Bejan, Entropy generation minimization, *J. Appl. Phys.*, 1996, **79**, 1191–1218.
32 B. Iftikhar, T. Javed and M. A. Siddiqu, Entropy generation analysis during MHD mixed convection flow of non-Newtonian fluid saturated inside the square cavity, *J. Comput. Sci.*, 2023, **66**, 101907.
33 T. Hayat, A. Razaq, S. A. Khan and A. Alsaedi, Entropy generation in chemically reactive and radiative Reiner-Rivlin fluid flow by stretching cylinder, *J. Magn. Magn. Mater.*, 2023, **573**, 170657.
34 H. Maiti, A. Y. Khan, S. Mondal and S. K. Nandy, Scrutinization of unsteady MHD fluid flow and entropy generation: hybrid nanofluid model, *Journal of Computational Mathematics and Data Science*, 2023, **6**, 100074.
35 A. Alsaedi, S. A. Khan and T. Hayat, A model development for thermal and solutal transport analysis in radiating entropy optimized and magnetized flow of nanomaterial by convectively heated stretched surface, *Chaos, Solitons Fractals*, 2023, **171**, 113424.
36 M. O. Oni and B. K. Jha, Entropy generation analysis of electroosmotic mixed convection flow in vertical microannulus with asymmetric heat fluxes, *Int. Commun. Heat Mass Transfer*, 2023, **145**, 106813.
37 L. S. Sundar and H. K. Mewada, Experimental entropy generation, exergy efficiency and thermal performance factor of $CoFe_2O_4$/water nanofluids in a tube predicted with ANFIS and MLP models, *Int. J. Therm. Sci.*, 2023, **190**, 108328.
38 H. Zhao, D. Zhao and S. Becker, Entropy production and enhanced thermal performance studies on counter-flow double-channel hydrogen/ammonia-fuelled micro-combustors with different shaped internal threads, *Int. J. Hydrogen Energy*, 2022, **47**, 36306–36322.
39 M. O. Oni and B. K. Jha, Entropy generation analysis of electroosmotic mixed convection flow in vertical microannulus with asymmetric heat fluxes, *Int. Commun. Heat Mass Transfer*, 2023, **145**, 106813.
40 T. Siva, S. Jangili and B. Kumbhakar, Entropy generation on EMHD transport of couple stress fluid with slip-dependent zeta potential under electrokinetic effects, *Int. J. Therm. Sci.*, 2023, **191**, 108339.
41 A. Ali, S. Sarkar, S. Das and R. N. Jana, A report on entropy generation and Arrhenius kinetics in magneto-bioconvective flow of cross nanofluid over a cylinder with wall slip, *Int. J. Ambient Energy*, 2022, DOI: **10.1080/01430750.2022.2031292**.
42 A. J. Chamkha and A. R. A. Khaled, Hydromagnetic combined heat and mass transfer by natural convection from a permeable surface embedded in a fluid-saturated

porous medium, *Int. J. Numer. Methods Heat Fluid Flow*, 2000, **10**, 455–477.

43 H. Waqas, F. F. Bukhari, U. Farooq, M. S. Alqarni and T. Muhammad, Numerical computation of melting heat transfer in nonlinear radiative flow of hybrid nanofluids due to permeable stretching curved surface, *Case Stud. Therm. Eng.*, 2021, **27**, 101348.

44 E. N. Maraj, Z. Khatoon, S. Ijaz and R. Mehmood, Effect of Arrhenius activation energy and medium porosity on mixed convective diluted ethylene glycol nanofluid flow towards a curved stretching surface, *Int. Commun. Heat Mass Transfer*, 2021, **129**, 105691.

45 A. J. Chamkha, Non-Darcy hydromagnetic free convection from a cone and a wedge in porous media, *Int. Commun. Heat Mass Transfer*, 1996, **23**, 875–887.

46 S. Das, A. Ali and R. N. Jana, Numerically framing the impact of magnetic field on nanofluid flow over a curved stretching surface with convective heating, *World J. Eng.*, 2021, **18**, 938–947.

47 M. V. Krishna and A. J. Chamkha, Hall and ion slip effects on MHD rotating boundary layer flow of nanofluid past an infinite vertical plate embedded in a porous medium, *Results Phys.*, 2019, **15**, 102652.

48 K. Hosseinzadeh, M. R. Mardani, M. Paikar, A. Hasibi, T. Tavangar, M. Nimafar, D. D. Ganji and M. B. Shafii, Investigation of second grade viscoelastic non-Newtonian nanofluid flow on the curve stretching surface in presence of MHD, *Results Eng.*, 2023, **17**, 100838.

49 A. Ali, R. N. Jana and S. Das, Radiative CNT-based hybrid magneto-nanoliquid flow over an extending curved surface with slippage and convective heating, *Heat Transfer*, 2021, **50**, 2997–3020.

50 H. Waqas, F. F. Bukhari, U. Farooq, M. S. Alqarni and T. Muhammad, Numerical computation of melting heat transfer in nonlinear radiative flow of hybrid nanofluids due to permeable stretching curved surface, *Case Stud. Therm. Eng.*, 2021, **27**, 101348.

51 T. Hayat, R. S. Saif, R. Ellahi, T. Muhammad and B. Ahmad, Numerical study for Darcy-Forchheimer flow due to a curved stretching surface with Cattaneo-Christov heat flux and homogeneous-heterogeneous reactions, *Results Phys.*, 2017, **7**, 2886–2892.

52 B. Ullah, B. M. Fadhl, B. M. Makhdoum, K. S. Nisar, H. A. Wahab and U. Khan, Heat transfer analysis in Darcy Forchheimer flow of hybrid nanofluid for multiple shape effects over a curved stretching surface, *Case Stud. Therm. Eng.*, 2022, **40**, 102538.

53 L. Zhang, M. M. Bhatti, E. E. Michaelides, M. Marin and R. Ellahi, Hybrid nanofluid flow towards an elastic surface with tantalum and nickel nanoparticles, under the influence of an induced magnetic field, *Eur. Phys. J.: Spec. Top.*, 2022, **231**, 521–533.

54 T. Hayat, A. Razaq, S. A. Khan and A. Alsaedi, An induced magnetic field utilization for hybrid nanoliquid flow subject to entropy generation, *J. Magn. Magn. Mater.*, 2023, **576**, 170742.

55 N. F. Okechi, M. Jalil and S. Asghar, Flow of viscous fluid along an exponentially stretching curved surface, *Results Phys.*, 2017, **7**, 2851–2854.